Acta Pharmaceutica Sinica B 2021;11(9):2670–2684

Chinese Pharmaceutical Association
Institute of Materia Medica, Chinese Academy of Medical Sciences

Acta Pharmaceutica Sinica B

www.elsevier.com/locate/apsb
www.sciencedirect.com

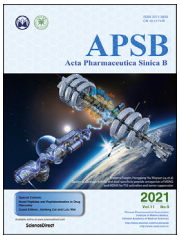

ORIGINAL ARTICLE

Apoptosis-inducing activity of synthetic hydrocarbon-stapled peptides in H358 cancer cells expressing KRAS^{G12C}

Cuicui Li[a,b], Ni Zhao[a,b], Luyan An[a,b], Zhen Dai[a,b], Xiaoyi Chen[a,b], Fan Yang[a,b], Qidong You[a], Bin Di[a,b,*], Chi Hu[c,*], Lili Xu[a,b,*]

[a]*Jiangsu Key Laboratory of Drug Design and Optimization, China Pharmaceutical University, Nanjing 210009, China*
[b]*Key Laboratory of Drug Quality Control and Pharmacovigilance, Ministry of Education, China Pharmaceutical University, Nanjing 210009, China*
[c]*Department of Pharmaceutical Engineering, School of Engineering, China Pharmaceutical University, Nanjing 211198, China*

Received 24 May 2021; received in revised form 16 June 2021; accepted 16 June 2021

KEY WORDS

Stapled peptides;
KRAS^{G12C};
Non-small cell lung cancer;
Stability;
Cell-cycle arrest and apoptosis

Abstract Lung cancers are the leading cause of cancer deaths worldwide and pose a grave threat to human life and health. Non-small cell lung cancer (NSCLC) is the most frequent malignancy occupying 80% of all lung cancer subtypes. Except for other mutations (*e.g.*, *KRAS*$^{G12V/D}$) that are also vital for the occurrence, *KRAS*^{G12C} gene mutation is a significant driving force of NSCLC, with a prevalence of approximately 14% of all NSCLC patients. However, there are only a few therapeutic drugs targeting KRAS^{G12C} mutations currently. Here, we synthesized hydrocarbon-stapled peptide **3** that was much shorter and more stable with modest KRAS^{G12C} binding affinity and the same anti-tumor effect based on the α-helical peptide mimic SAH-SOS1$_A$. The stapled peptide **3** effectively induced G2/M arrest and apoptosis, inhibiting cell growth in KRAS-mutated lung cancer cells *via* disrupting the KRAS-mediated RAF/MEK/ERK signaling, which was verified from the perspective of genomics and proteomics. Peptide **3** also exhibited strong anti-trypsin and anti-chymotrypsin abilities, as well as good plasma stability and human liver microsomal metabolic stability. Overall, peptide **3** retains the equivalent anti-tumor activity of SAH-SOS1$_A$ but with improved stability and affinity, superior to SAH-SOS1$_A$. Our work offers a structural optimization approach of KRAS^{G12C} peptide inhibitors for cancer therapy.

*Corresponding authors. Tel./fax: +86 25 83271269.
E-mail addresses: dibin@cpu.edu.cn (Bin Di), chihu@cpu.edu.cn (Chi Hu), 1620174420@cpu.edu.cn (Lili Xu).

Peer review under responsibility of Chinese Pharmaceutical Association and Institute of Materia Medica, Chinese Academy of Medical Sciences.

https://doi.org/10.1016/j.apsb.2021.06.013

1. Introduction

Till now, lung cancers remain the top cancer killer worldwide, afflicting millions of people with low quality of life today[1,2]. Although diagnostics and treatments have been upgrading, its prevalence still necessitates more attention to better treatment for improved survival[3]. Non-small cell lung cancer (NSCLC) occupy approximately 80% of all lung cancer subtypes[4]. Mutations of the rat sarcoma (*RAS*) gene family, a group of essential proto-oncogenes, are frequently detected in NSCLC patients[5,6], with constitutively active mutations observed in nearly one-third of human tumors. Kirsten rat sarcoma 2 viral oncogene homolog (*KRAS*) gene mutations comprise 90% of all oncogenic mutations in RAS in lung adenocarcinoma[7,8]. Known carcinogenic *RAS* mutations may disrupt the RAS guanosine triphosphatases (GTPase) activities and impair guanosine triphosphate (GTP) hydrolysis, leading to RAS protein accumulation in the active GTP-binding form and subsequently enhancing downstream signaling activities[9]. Three strategies directly target *RAS* genes: (i) a covalent inhibitor of the oncogenic mutant $KRAS^{G12C}$ Cys12, (ii) disrupting the downstream signalings by interfering with RAS–effector interactions[10], (iii) inhibiting RAS–guanine nucleotide exchange factor (GEF) interactions to prevent GTP overload[11,12]. Notably, several $KRAS^{G12C}$ covalent inhibitors have been successfully used in a recent screening based on disulfide fragment to identify small molecules that can covalently modify the mutant more precisely. Two of them, AMG510 and MRTX849, have exhibited promising response rates in clinical trials of $KRAS^{G12C}$-driven lung adenocarcinoma[9,13,14].

KRAS mutations at residues 12, 13, or 61, which induce KRAS translation, are involved in the carcinogenic process[52], where in mutations are prevalent at residues 12 and 13 in NSCLC, account for 97%[50], particularly at residue 12 (80%)[51]. Membrane-bound RAS proteins act as a molecular switch in vital signaling pathways[15], regulating cell proliferation, differentiation, metabolism, survival, and other life processes by converting between GDP-binding and GTP-binding conformations (RAS-GDP and RAS-GTP) through GTPase activating protein (GAP) and GEF[16]. Son of sevenless 1/2 (SOS1/2) are one of the members of GEFs[17]. SOS inserts α-helical hairpin, a crucial factor of this catalytic process, into the switch regions of RAS, disrupting the interaction between RAS and guanine nucleotide[18,19]. Hence, we are very interested in the development of inhibitors that interfere with the $KRAS^{G12C}$/SOS interaction.

The α-helix secondary structure in the folded subdomain of the protein−protein interaction constitutes the supporting backbone. Special α-helix fragment can be extracted separately to chemically synthesize an active polypeptide drug that selectively acts on KRAS proteins[20]. Its large size and strong ability to span large contact areas make it suitable to inhibit RAS protein, a compelling but challenging drug target[21]. To interfere with the KRAS–SOS1 interaction, Leshchiner et al.[18] designed SAH-$SOS1_A$, an 18-residue stapled peptide, by introducing an i,i+4 hydrocarbon linker on the non-interacting face of the SOS1 α-helix (F929−N944) and adding two arginines at the N-terminus. Common polypeptide fragments are prone to form random coil conformation, resulting in weaker binding and susceptibility to degradation by peptidases. The side chain of the cyclic, full-carbon skeleton can stabilize the active conformation of the α-helical peptide. Stapled peptides overcome the defect that the polypeptide fragments isolated from the whole protein structure cannot form the secondary structure required for binding[22−26].

Most polypeptide drugs on the market are about ten amino acids in length, and their low solubility, poor stability, and high cost restrict novel polypeptide development. In this study, we aimed to structurally modify SAH-$SOS1_A$ to improve its anti-tumor activity, binding affinity, stability, etc. Since $KRAS^{G12C}$ mutational activation has been proven critical in NSCLC occurrence, we hope to offer a new case for more efficient designs of peptidomimetics and non-peptide drugs against other cancer types.

2. Results

2.1. Design and synthesis of stapled peptides

A longer sequence brings about low solubility and poor stability of peptide drugs with higher production costs, being obstacles in peptide drug research and development. Most peptide drugs on the market are composed of about ten amino acids in length to circumvent this conundrum, for example, octreotide[27]. SAH-$SOS1_A$, a stapled peptide with 18 residues, has the potential to be simplified into a shorter α-helical stapled peptide. The most effective strategy for structural simplification of peptides is to shorten the length of peptides systematically.

SAH-$SOS1_A$ was designed by Leshchiner et al.[18] and became the basis of numerous new stapled peptides synthesized since then. In this paper, SAH-$SOS1_A$ used as the positive peptide was designated as peptide **1**, which provided a reference for testing other peptides. In order to obtain shorter peptides, we first tried to truncate the amino acid residues with low hydrophobicity at both ends: three amino acid residues were truncated from the C-terminus, and two were truncated from the N-terminus to obtain peptide **2**. While the affinity of peptide **2** targeting the $KRAS^{G12C}$ protein was slightly improved, there was nowhere to near the formation of the α-helical structure. So, two more amino acid residues at both ends of peptide **2** were truncated to obtain peptide **3**. The affinity analysis showed that compared with the positive peptide, the affinity of peptide **3** to $KRAS^{G12C}$ protein had been greatly improved, with a better α-helical structure. We found that shortening the peptide at N- or C-terminal end was indeed useful for improving affinity. Peptides **4**−**6** were subsequently designed based on the same idea. However, they were unable to form an α-helical structure due to a small number of amino acids. So, we modified the current strategy by truncating the N-terminal amino acid while retaining the C-terminal amino acid based on peptide **3** to obtain peptides **7**−**8**, and then truncating the C-terminal amino acid but maintaining the N-terminal amino acid to obtain peptides **9**−**10**.

Finally, we designed and synthesized ten peptides, including SAH-$SOS1_A$, as shown in Table 1. The N-terminus of these peptides was acetylated while C-terminus was amidated. The solid-phase synthesis of stapled peptides was performed as described elsewhere[28] (Fig. 1). Two unnatural amino acids that contain α-methyl, α-alkenyl side chains were introduced into the peptide and the staple covalently formed by Grubbs' 2nd-generation catalyst-catalyzed ring-closing metathesis[9].

2.2. Characterization of the secondary structure of stapled peptides

We examined the α-helical structures of peptides **1**−**10** by circular dichroism (CD) spectroscopy to confirm whether shortening the length of the stapled peptides could affect the α-helical structure[29]. CD has been widely applied for characterizing the secondary structure of proteins and peptides with

the advantages of simple sample preparation, rapid and non-destructive analysis. The structural potential of the stapled peptides was further assessed using 2,2,2-trifluoroethanol (TFE), a solvent that promotes the helix formation of intrinsically helical motifs. Generally, the CD spectra of peptides with a typical secondary structure are plotted into the far-ultraviolet range (185−245 nm).

It was observed from Fig. 2A and B that in PBS, most of the stapled peptides revealed a random coil conformation, but peptides **1**, **3**, and **7** showed the circular dichroic spectral characteristics of α-helical conformation, whose α-helicity was 16.20%, 18.93%, and 17.90%, respectively. In PBS containing 50% TFE, the increased helicity was observed in the majority of the peptides, showing the potential to form the α-helical structure. Peptides **1**, **3**, **7**, and **9** had higher α-helicity of 33.84%, 43.75%, 22.10%, and 20.60%, respectively. The α-helicity of other peptides was lower than 10% (Fig. 2C and D).

Overall, peptide **3** exhibited a better α-helical conformation among all stapled peptides, with the greatest potential to form α-helical conformation.

2.3. *The binding affinity of stapled peptides to KRAS^{G12C} protein*

To determine the direct binding of stapled peptides to KRAS^{G12C} protein, a label-free, real-time binding assay of biomolecular interactions was performed with Fortebio's Bio-Layer Interferometry (BLI) technology. Binding affinity is measured by equilibrium dissociation constant to determine the strength of biomolecular interactions.

As shown in Supporting Information Fig. S1, peptides **1** and **2** had a fast association rate and a rapid dissociation rate, while peptides **3**, **4**, **6**−**8**, and **10** bound to KRAS^{G12C} protein with a slow association rate and a slow dissociation rate. Peptide **9** exhibited a slow association rate and a rapid dissociation rate; peptide **5** not only had a low binding signal value but also showed abnormalities in the association−dissociation curve. The K_D value of the positive peptide **1** was 58.3 μmol/L, and those of peptides **2**−**4**, and **8** were 21.7, 7.67, 25, and 29.1 μmol/L, respectively. The affinity of peptides **2**−**4**, and **8** to KRAS^{G12C} protein was higher compared with peptide **1**. The K_D values of peptides **7**, **9**, and **10** were 87.2, 64.9, and 131 μmol/L, respectively, and their affinity to KRAS^{G12C} protein was lower compared with the positive peptide. The K_D values for the affinity of peptides **5** and **6** to KRAS^{G12C} protein were in the millimolar order (Table 2).

Peptide **3** had the highest affinity for KRAS^{G12C} protein in all of those stapled peptides, with a slower association rate and a slower dissociation rate, superior to the positive peptide **1**. The positive peptide **1** had a faster association rate and a faster dissociation rate *versus* peptide **3**, explaining a more stable binding of the stapled peptide **3** to KRAS^{G12C} protein.

In order to further confirm the conclusion that peptide **3** is superior to the positive peptide **1**, we evaluated the binding affinity of the stapled peptides to KRAS^{G12C} protein using optimized fluorescence polarization (FP) binding assay. Firstly, the working concentrations of FITC-Peptide-**1** and FITC-Peptide-**3** were optimized. As shown in Supporting Information Fig. S2A, as the concentration of the fluorescent probe increased, the fluorescence polarization value gradually decreased and eventually stabilized. Hence, 125 and 62.5 nmol/L were selected as the best working concentrations of FITC-Peptide-**1** and FITC-Peptide-**3**, respectively. It can be seen from Fig. S2B that as the concentration of KRAS^{G12C} protein increased, the fluorescence polarization value gradually increased and finally stabilized. Among them, the EC_{50} value of FITC-Peptide-**1** binding to KRAS^{G12C} protein was 6.344 μmol/L, while the EC_{50} value of FITC-Peptide-**3** binding to KRAS^{G12C} protein was 1.359 μmol/L. The results of this experiment once again proved that the affinity of peptide **3** to KRAS^{G12C} protein was higher than that of the positive peptide **1**.

2.4. *The stapled peptide **3** interacted with Cys12 of KRAS^{G12C} through hydrophobic interaction*

We subsequently investigated the interaction mode of peptides **1** and **3** with KRAS^{G12C} protein (Fig. 3). The docking analysis indicated that peptide **1** interacted with Ala59, Gly60, Gln61, Tyr64, and Tyr71 of KRAS^{G12C} protein through hydrophobic interactions and hydrogen-bond interactions. Peptide **3** interacted with Cys12, Val14, Gly15, Lys16, Asp57, Ala59, Gly60, Gln61, and Glu63 of KRAS^{G12C} protein through electrostatic, hydrogen-bond, and hydrophobic interactions.

Comparing the binding interaction of peptide **1** *versus* peptide **3** with KRAS^{G12C} protein, more amino acids joined the interactions between peptide **3** and KRAS^{G12C} protein. Based on docking analysis, peptide **3** interacted with Cys12 of KRAS^{G12C} protein through hydrophobic interactions, but no interaction between peptide **1** and Cys12 was observed. Therefore, we speculate that this is one reason for the higher affinity-binding of peptide **3** to target protein than that of peptide **1**.

Table 1 Physicochemical properties of the designed stapled peptides.

Peptide	Sequence	L	NC	PR/*n*%	NPR/*n*%
1	Ac-RRFFGIS$_5$LTNS$_5$LKTEEGN-NH$_2$	18	+1	11/61.1	7/38.9
2	Ac-FFGIS$_5$LTNS$_5$LKTE-NH$_2$	13	0	6/46.2	7/53.8
3	Ac-FGIS$_5$LTNS$_5$LKT-NH$_2$	11	+1	5/45.5	6/54.5
4	Ac-GIS$_5$LTNS$_5$LK-NH$_2$	9	+1	4/44.4	5/55.6
5	Ac-IS$_5$LTNS$_5$L-NH$_2$	7	0	2/28.6	5/71.4
6	Ac-S$_5$LTNS$_5$-NH$_2$	5	0	2/40.0	3/60.0
7	Ac-IS$_5$LTNS$_5$LKT-NH$_2$	9	+1	4/44.4	5/55.6
8	Ac-S$_5$LTNS$_5$LKT-NH$_2$	8	+1	4/50.0	4/50.0
9	Ac-FGIS$_5$LTNS$_5$L-NH$_2$	9	0	3/33.3	6/66.7
10	Ac-FGIS$_5$LTNS$_5$-NH$_2$	8	0	3/37.5	5/62.5

S$_5$: (*S*)-α-Methyl-α-pentenyl glycine; L, length; NC, net charge; PR, number of polar residues; NPR, number of nonpolar residues.

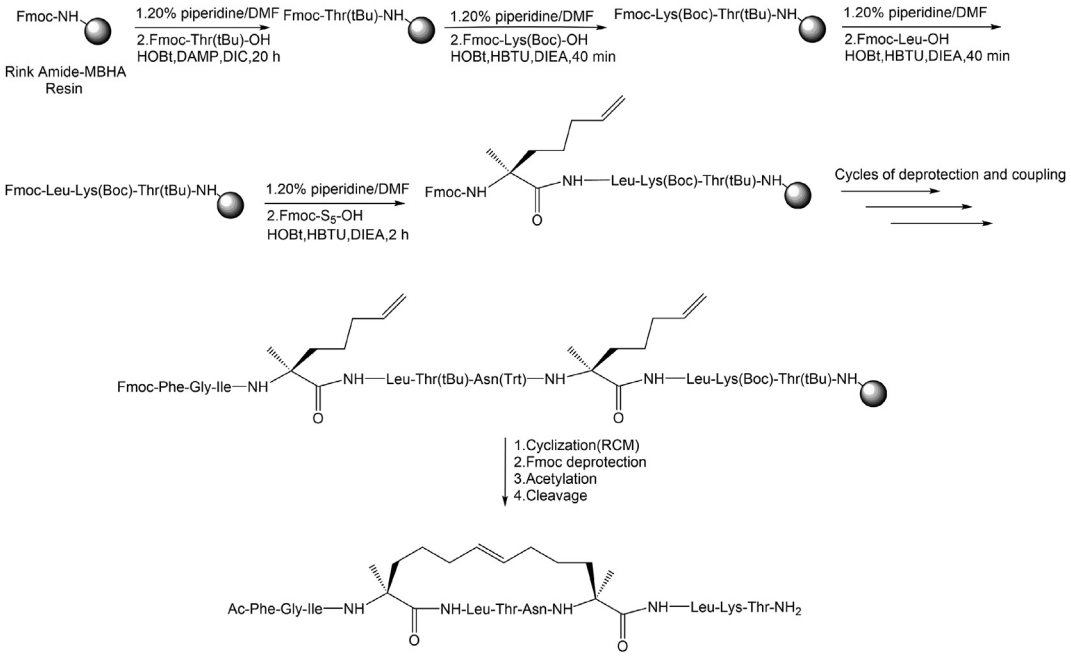

Figure 1 Solid-phase peptide synthesis of hydrocarbon-stapled peptide **3**. Other stapled peptides were synthesized in the same way. α-Methyl, α-alkenyl glycine cross-linking amino acids were incorporated as shown to synthesize stapled peptides.

2.5. *The stapled peptide **3** directly inhibited the binding of KRAS^{G12C} to GDP*

The stapled peptide **3** inhibited the binding of KRAS^{G12C} to GDP in a concentration-dependent manner *in vitro*. KRAS^{G12C} and equimolar fluorescence GDP analog mant-GDP were used as a positive control. Excess unlabeled GDP (200X) was used as a negative control. KRAS^{G12C} was then co-incubated with mant-GDP and peptide **1** or **3**. The decrease of relative fluorescence values observed in the same curve reflects the conversion activity of GDP in the KRAS^{G12C} active site. In the different curves, the higher relative fluorescence value represents the stronger inhibition of KRAS^{G12C} and GDP binding. As shown in Fig. 4A and B, both peptides **1** and **3** inhibited mant-GDP binding in a concentration-dependent manner, the effect of peptide **3** was equivalent to that of peptide **1**. Therefore, the results indicated that peptide **3** can directly inhibit the binding of KRAS^{G12C} to GDP as well as peptide **1**.

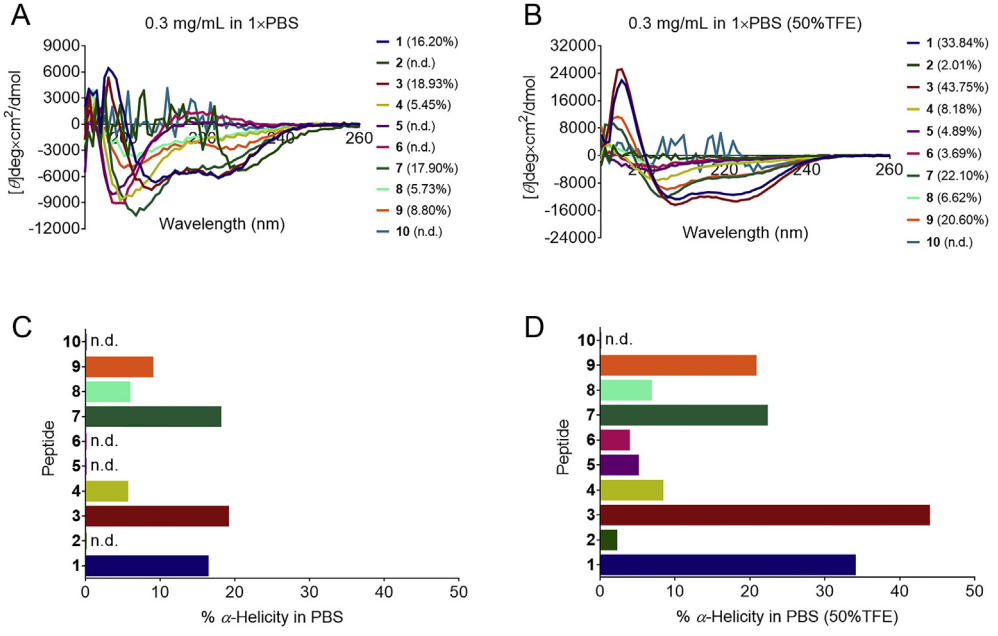

Figure 2 (A) CD spectra of stapled peptides in the range of 190−260 nm in PBS. (B) α-Helicity of stapled peptides in PBS. (C) CD spectra of stapled peptides in the range of 190−260 nm in PBS (50% TFE). (D) α-Helicity of stapled peptides in PBS (50% TFE). n.d.: not determined.

Table 2 Kinetics of interaction of peptides with $KRAS^{G12C}$ protein determined by BLI.

Peptide	Sequence	K_D (mol/L)	K_{on} (L/mol·s)	K_d (s^{-1})
1	Ac-RRFFGIS$_5$LTNS$_5$LKTEEGN-NH_2	5.83E−05	1.48E+04	8.62E−01
2	Ac-FFGIS$_5$LTNS$_5$LKTE-NH_2	2.17E−05	4.36E+04	9.46E−01
3	Ac-FGIS$_5$LTNS$_5$LKT-NH_2	7.67E−06	4.60E+03	3.53E−02
4	Ac-GIS$_5$LTNS$_5$LK-NH_2	2.50E−05	9.76E+01	2.44E−03
5	Ac-IS$_5$LTNS$_5$L-NH_2	3.40E−01	3.12E+00	1.06E+00
6	Ac-S$_5$LTNS$_5$-NH_2	6.11E−02	3.22E+00	1.97E−01
7	Ac-IS$_5$LTNS$_5$LKT-NH_2	8.72E−05	6.47E+01	5.64E−03
8	Ac-S$_5$LTNS$_5$LKT-NH_2	2.91E−05	1.75E+03	5.09E−02
9	Ac-FGIS$_5$LTNS$_5$L-NH_2	6.49E−05	1.63E+03	1.06E−01
10	Ac-FGIS$_5$LTNS$_5$-NH_2	1.31E−04	2.94E+02	3.85E−02

2.6. *Viability of H358 cells treated with stapled peptides*

We assessed the viability of H358 cells after incubation with a diluted series of the stapled peptides. As is evident from Fig. 4C and D, the inhibition of H358 cell proliferation induced by peptides **1** and **3** was most potent, followed by peptide **2**. However, no noticeable inhibition was observed for the other stapled peptides over the concentration range studied. The inhibitory effect of stapled peptide **3** (IC_{50} = 15.69 μmol/L) was comparable to that of the positive peptide **1** (IC_{50} = 21.25 μmol/L). To further confirm the cell proliferation inhibitory activity of peptide **3**, we extended its treatment time. As shown in Supporting Information Fig. S3, after 36, 48, and 72-h incubation, the IC_{50} of peptide **3** was 7.546, 5.749, and 6.680 μmol/L, respectively, which showed the stability of peptide **3** in cancer cell within 72 h.

After a comprehensive analysis of the secondary structure, cellular viability and affinity of all stapled peptides shortened, peptide **3** exhibited the highest α-helicity, the best cellular viability, and the modest affinity to the $KRAS^{G12C}$ protein. Therefore, the stapled peptide **3** was selected for further analysis.

2.7. *The stapled peptide **3** induced G2/M arrest in H358 cells*

The survival rate of $KRAS^{G12C}$ mutant cell line H358 was decreased in a concentration-dependent characteristic after incubation with peptide **3**, as indicated by the CCK8 assay. Two underlying mechanisms may result in this effect: (1) inducing cell autophagy, apoptosis, necrosis, or other cell death pathways; (2) interfering with the cell cycle to lead to failure of cell proliferation. To investigate how the stapled peptide **3** suppressed H358 cell survival and whether it has any effects on cell cycle, we measured the cell-cycle distribution of H358 cells by flow cytometry. The results showed a noticeable increase in the percentage of the G2/M phase with increasing concentration of peptide **3** after 24-h treatment. As shown in Fig. 5A and B, the percentage of cells in the G2/M rose from 16.76% to 49.79%, indicating that peptide **3** induced H358 cells G2/M-phase cell-cycle arrest. Furthermore, we evaluated the effect of peptide **3** on G2/M-related protein expressions using Western blot to get a better understanding of how peptide **3** induced G2/M arrest in H358 cells. As shown in Fig. 5E, cyclin B1 and cyclin-dependent kinase 1 (CDK1) expressions (key proteins in the G2 to M phase transition) were significantly downregulated with peptide **3**, indicating that peptide **3**-induced H358 cells G2/M arrest may be attributed to its effect on CDK1 and cyclin B1, resulting in the inhibition of cell proliferation.

2.8. *The stapled peptide **3** induced apoptosis in H358 cells*

To determine whether the loss of H358 cell proliferation is associated with the peptide **3**-mediated cell apoptosis, apoptosis was evaluated by flow cytometry. As shown in Fig. 5C and D, the proportion of apoptotic cells in peptide **3**-treated H358 cells were 56.63%, 61.40%, and 70.70% at the concentration of 2.5, 10, and 20 μmol/L, respectively, significantly higher compared with the control group (36.42%). Peptide **3** increased apoptosis of H358 cells in a dose-dependent characteristic. The mechanisms of how peptide **3** mediated apoptosis were explored *via* determining the expressions of several characterized apoptotic proteins using Western blot. As shown in Fig. 5F, peptide **3** exerted a insignificant effect on pro-apoptotic BAX protein expression. But the expression of anti-apoptotic BCL-2 protein was obviously inhibited, and the expression of caspase 3 increased in H358 cells. As the balance between pro- and anti-apoptotic molecules determines the apoptosis outcome, peptide **3** may induce H358 cell apoptosis *via* disrupting the BCL-2/BAX ratio.

2.9. *The stapled peptide **3** inhibited KRAS downstream phosphosignaling*

Growth factor-mediated KRAS activation is known to activate the RAF/MEK/ERK pathway, the key downstream signaling of KRAS[30]. We examined the effect of peptide **3** on the phosphorylation status of extracellular signal-regulated kinase (ERK) in H358 cells using Western blot to determine whether peptide **3**-mediated inhibition on H358 cell viability was KRAS-dependent[18,31]. The results showed that treatment with peptide **3** dose-responsively inhibited ERK1/2 phosphorylation in H358 cells (Fig. 5G), without any effect on total ERK1/2. Our data indicated that peptide **3** inhibited H358 cell growth and survival by regulating KRAS downstream phosphosignaling.

Above all, peptide **3** could induce G2/M arrest and apoptosis to inhibit H358 cell growth by disrupting the KRAS-mediated RAF/MEK/ERK signaling pathway (Fig. 5).

2.10. *Genomics analysis in peptide **3** treatment of H358 cells*

We investigated the underlying mechanism of peptide **3** exhibited anti-tumor performance. Using PBS treatment as a blank control, we so performed RNA sequencing of H358 cells after peptide **3** treatment. A heatmap of genes that were differentially expressed in H358 cells after treatment was generated from RNA sequencing (Fig. 6A). Compared with the control group, the

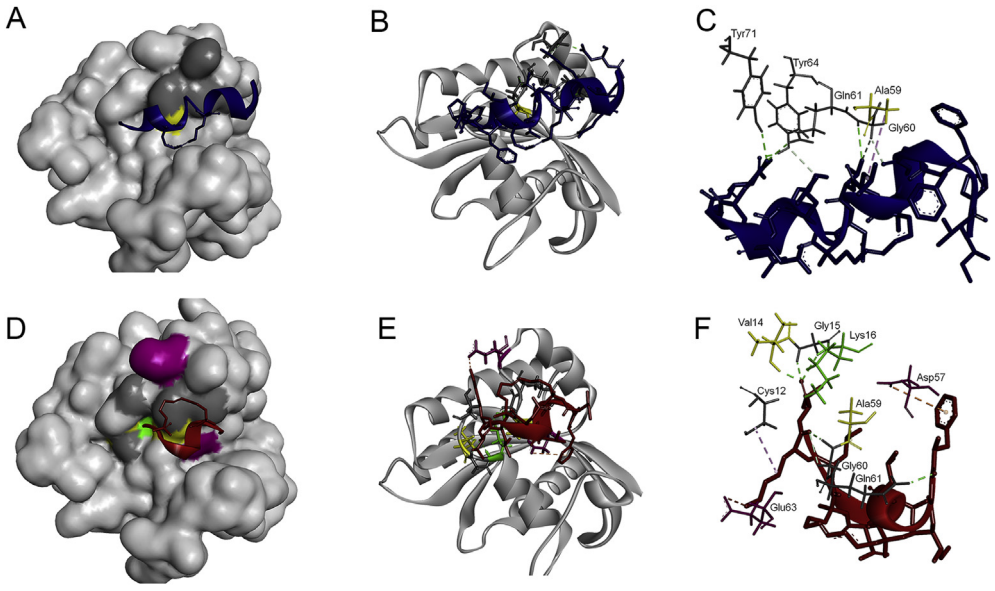

Figure 3 (A)−(C) Binding interactions of the positive peptide **1** (blue helix) with KRAS^{G12C} protein (light grey surface). (D)–(F) Binding interactions of the stapled peptide **3** (red helix) with KRAS^{G12C} protein (light grey surface). The starting structural model PDB ID code is 6EPL. Amino acid residues at the interaction interface of KRAS^{G12C} protein are colored according to their physicochemical properties (purple = negative, green = positive, yellow = hydrophobic, and grey = hydrophilic).

expression levels of 185 genes were significantly altered following peptide **3** treatment. Among these differentially expressed genes, 115 genes were downregulated, and 70 genes were upregulated (Fig. 6B). As shown in Fig. 6C, Kyoto Encyclopedia of Genes and Genomes (KEGG) analysis showed that differentially expressed genes after peptide **3** treatment were involved in various signaling pathways including the RAS signaling pathway, which was further confirmed that peptide **3** could induce H358 cells apoptosis through KRAS-mediated signaling pathway.

2.11. Quantitative proteomics analysis based on tandem mass tag (TMT)

The differential expression proteins between control and treatment samples could more exactly reflect the proteomic changes induced by peptide **3**. Therefore, TMT quantitative proteomic analysis was performed and focused on the proteome alteration of H358 cells after peptide **3** treatment. A total of 49,703 unique peptides and 7012 protein groups were identified and annotated in all samples. A heatmap of proteins that were differentially expressed in H358 cells after

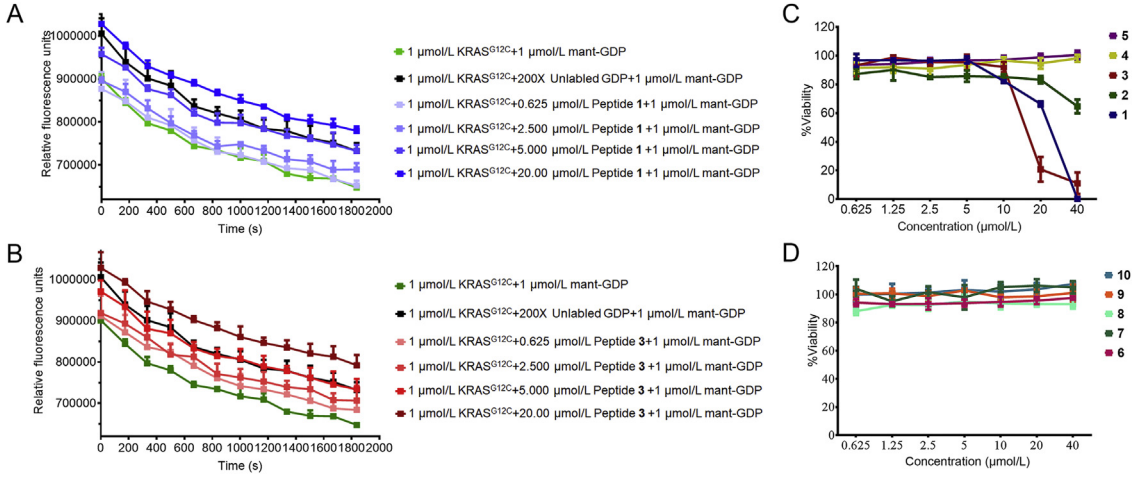

Figure 4 Peptide **1** (A) and **3** (B) inhibited nucleotide association with KRAS^{G12C}. Mant-GDP was incubated with KRAS^{G12C} protein and the decrease in fluorescence was monitored over time (green). Coincubation with unlabeled nucleotide served as a negative control (black). A serial dilution of peptides **1** and **3** was coincubated with KRAS^{G12C} and mant-GDP to monitor for effects on nucleotide association. (C)−(D) Cell viability of H358 cells after 24-h incubation with a diluted series of stapled peptides using the CCK8 assay. All data are shown as the mean ± SD of three independent experiments (n = 3).

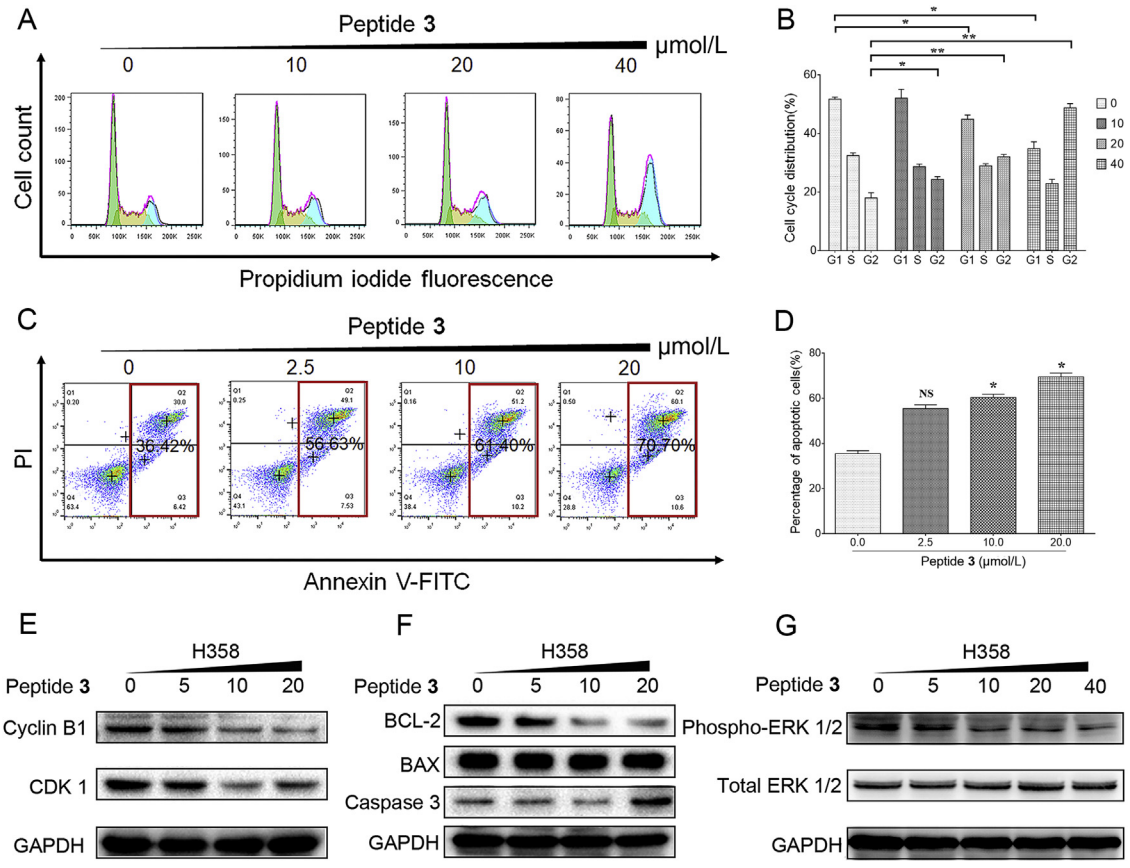

Figure 5 (A) Cell cycle distribution analysis of H358 cells by flow cytometry. H358 cells were treated with various concentrations of peptide **3** for 24 h. (B) The bar diagram depicted cell distribution in different phases of the cell cycle in H358 cells. $*P < 0.05$, $**P < 0.01$, the data were tested by one-way ANOVA. And the data shown represent results of three individual experiments ($n = 3$). (C) H358 cells were incubated with peptide **3** for 24 h. Q1–4 represent the necrotic, late apoptotic, early apoptotic, and normal cells, respectively. The apoptotic ratio is represented by the summation of Q2 and Q3. (D) The bar diagram illustrates the proportion of apoptotic cells in H358 cells. $*P < 0.05$, $**P < 0.01$ (one-way ANOVA). The data shown represent results of three individual experiments ($n = 3$). (E) Western blot analysis of cycle-associated proteins. H358 cells were incubated with 0, 5, 10, 20 μmol/L peptide **3** for 24 h. The expressions of CDK1 and cyclin B1 protein were determined by Western blot. (F) Western blot analysis of proteins related to apoptosis. H358 cells were treated with 0, 5, 10, 20 μmol/L peptide **3** for 24 h. The expressions of caspase 3, BCL-2, and BAX protein were evaluated by Western blot. (G) Peptide **3** inhibited the downstream phosphosignaling proteins of KRAS *in vitro*. H358 cells were treated with the stapled peptide **3** (0, 5, 10, 20 and 40 μmol/L) for 24 h. Western blot analysis was conducted with antibodies specific for phospho- and total ERK1/2.

treatment was generated (Fig. 7A). Functional enrichment analysis, including KEGG and Gene Ontology (GO) analysis, was conducted for comprehensively understanding the functions of the differential expression proteins. Through KEGG enrichment analysis, differential expressed proteins after peptide **3** treatment were involved in various signaling pathways including the RAS signaling pathway (Fig. 7B). According to the GO enrichment statistics, the top GO terms in Biological Process were involved in apoptotic process and cell cycle; cell part was the most common Cellular Component term; protein binding among Molecular Function was the most abundant GO term (Fig. 7C). All of these were confirmed that peptide **3** could induce H358 cells apoptosis and cell cycle arrest through KRAS-mediated signaling pathway.

*2.12. The stapled peptide **3** exhibited extraordinary enzymatic stability*

The tendency of forming random coil conformations and degradation-susceptible property of peptide fragments in the absence of whole protein structure practically thwart the application of peptide drugs. Therefore, we examined the enzymatic stability of peptides **1** and **3**. Trypsin and chymotrypsin are abundant in the digestive system of mammals, hence, the susceptibility of peptides **1** and **3** to enzymatic degradation was examined in NH_4HCO_3 buffer at 37 °C with trypsin or chymotrypsin. The enzymatic degradation of peptides **1** and **3** was revealed on HPLC chromatograms[32,33].

Trypsin cleaves peptides mainly on the carboxyl side of arginine or lysine amino acid[34]. It was observed in Fig. 8A and C that peptide **1** (a) was enzymatically digested after adding trypsin, and the chromatographic peak area of its trypsin hydrolysate (b) was gradually decreased after incubating in trypsin for a certain period of time. The chromatographic peak area of peptide **3** (f) continued to decrease as the degradation progressed. 6% of peptide **3** remained undegraded after 24 h of degradation, and its trypsin hydrolysate (g) reached 78% at 12 h and decreased to 34% at 24 h, indicating that the trypsin hydrolysate of peptide **3** was degraded again.

It is known that chymotrypsin give priority to cleave peptide amide bonds on the carboxyl side of tryptophan, tyrosine, or

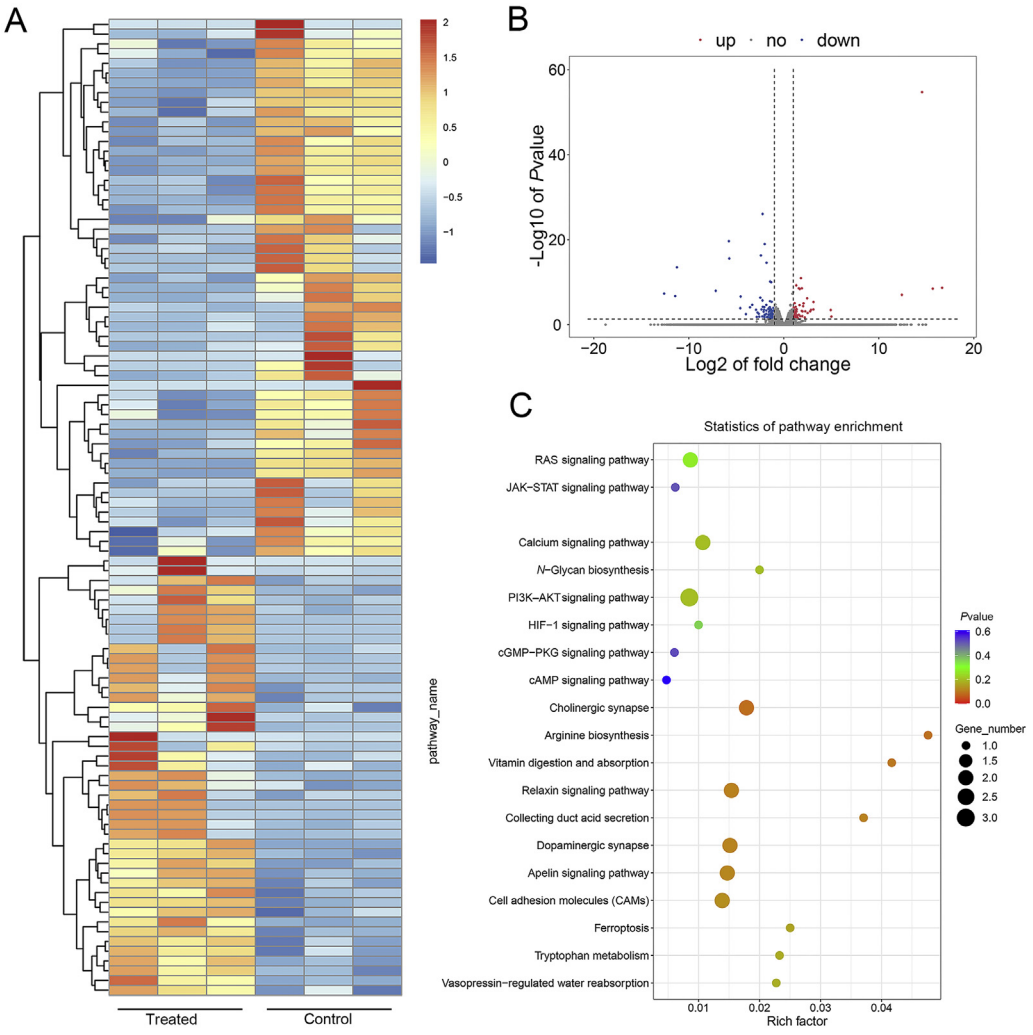

Figure 6 Heatmap (A) and volcano plots (B) of differentially expressed genes in H358 cells. (C) KEGG enrichment of signaling pathways in peptide **3**-treated H358 cells. The dot represents gene number.

phenylalanine residues[34]. Similarly, it was observed in Fig. 8D and F that peptide **1** (a) was enzymatically hydrolyzed after adding chymotrypsin, and the chromatographic peak area of the chymotrypsin hydrolysate (c–e) varies with the incubation time. The decrease in the chromatographic peak area of peptide **3** (f) persisted as degradation progressed, and 70% of peptide **3** remained undegraded at 24 h. While no obvious characteristic chromatographic peaks of peptide **3** chymotrypsin hydrolysates were observed.

The ExPASy PeptideCutter program was utilized to predict the digestion sites of peptides **1** and **3**. As PeptideCutter is only limited to natural amino acids, the peptide sequence RRFFGIYLTNILK-TEEGN was selected to simulate tryptic and chymotryptic digests. The highly specific cleavage sites of chymotrypsin were predicted to be located on the carboxyl side of phenylalanine and tyrosine. The low-specific cleavage sites of chymotrypsin were situated on the carboxyl side of phenylalanine, tyrosine, and leucine residues. The cleavage site of trypsin was located on the carboxyl side of lysine residue (Fig. 8G). Therefore, it is speculated that the action sites of trypsin in peptide **1** were located on the carboxyl side of lysine and arginine, while the cleavage sites of chymotrypsin were located on the carboxyl side of phenylalanine and leucine. And the possible tryptic and chymotryptic cleavage sites in peptide **3** were on the carboxyl side of lysine, and phenylalanine and leucine, respectively (Fig. 8H).

In summary, compared with the positive peptide **1**, peptide **3** showed stronger protease resistance in both trypsin and chymotrypsin. Furthermore, peptide **3** was more stable in chymotrypsin compared with trypsin.

*2.13. The stapled peptide **3** had better plasma stability and liver microsomal metabolic stability*

Since enzymatic hydrolysis stability has been found excellent in peptide **3**, it is worthy of investigating the plasma stability to assess the degradation of peptide **3** in the plasma. The plasma stability analysis of both peptides **1** and **3** following time-dependent incubation in rat plasma was carried out. As shown in Fig. 9A, the retention times of the characteristic peaks of peptides **1** and **3** in the HPLC chromatogram were 16.099 and 21.241 min, respectively. No characteristic peaks were observed in

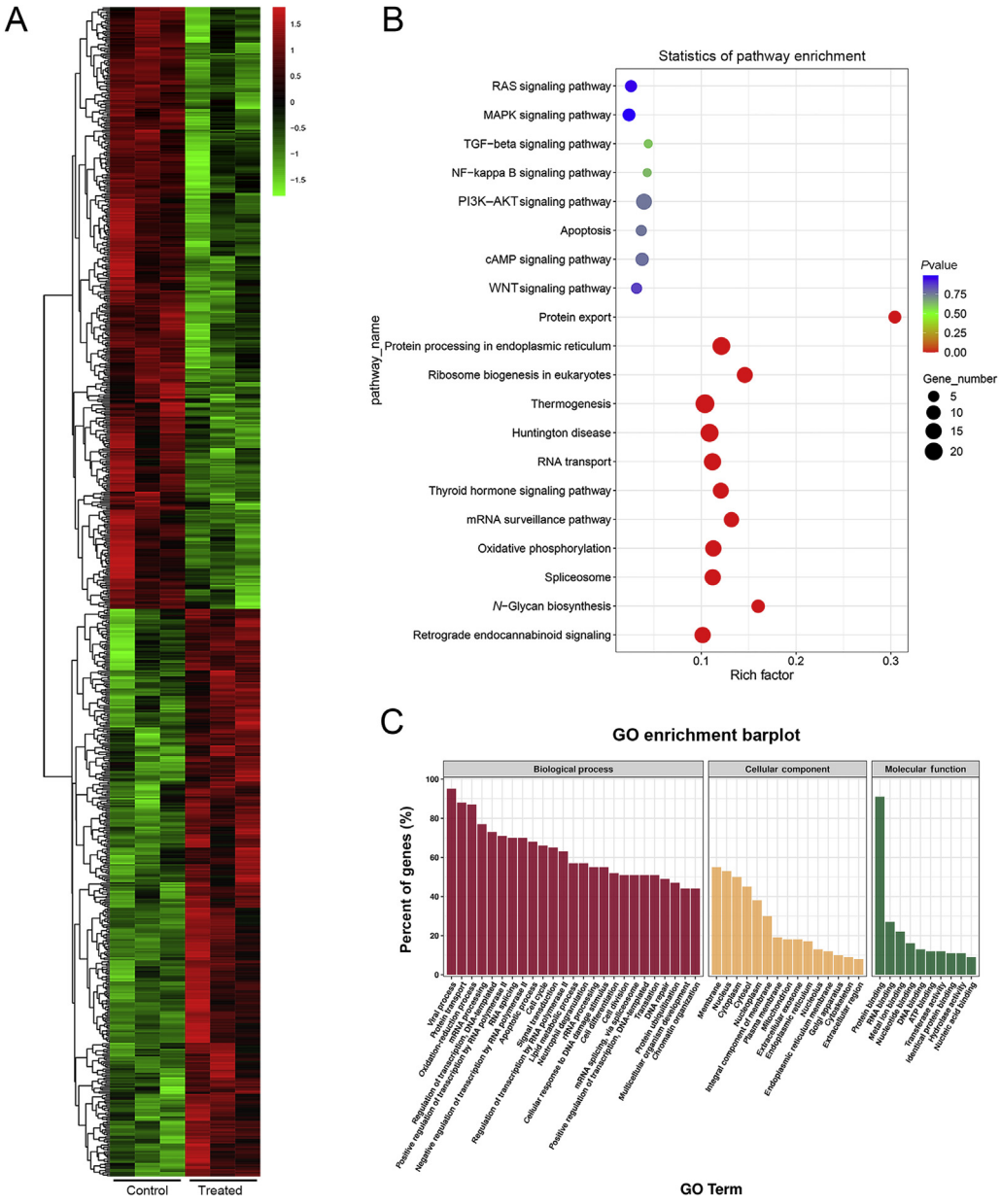

Figure 7 (A) Heatmap of differentially expressed proteins in H358 cells. (B) KEGG enrichment of signaling pathways in peptide **3**-treated H358 cells. The dot represents gene number. (C) GO enrichment of differentially expressed proteins in H358 cells.

the chromatogram of peptide **1** incubated in the plasma for 0 min (Fig. 9B and C). The characteristic peaks demonstrated that peptide **3** was stable in rat plasma (Fig. 9D and E). However, the percentage of the chromatographic peak area of peptide **3** did not show a downward trend within 480 min, indicating that peptide **3** was relatively stable in rat plasma.

The liver is an important organ for drug metabolism and the main place for biological transformation of the body, which contains various enzymes involved in phase I and II metabolism. Liver microsomes contain most of the phase I enzymes, of which the most important is the microsomal mixed-function oxidase system with CYP450 as the main component. Adding the corresponding cofactor NADPH to the liver microsomes can reorganize the *in vitro* metabolism system, so that the phase I metabolic stability study can be carried out by *in vitro* incubation method. We evaluated the metabolic stability of peptide **3** in liver microsomes and found that there was no obvious downward trend of the chromatographic peak area percentage within 300 min of incubation in human liver microsomes (Fig. 9F), indicating that peptide **3** was relatively stable in liver microsomes.

3. Discussion and conclusions

RAS is one of the most pervasive pathogenic factors in human cancers[18]. As aberrant RAS signaling has been confirmed to fuel the development of numerous cancers, drugs directly blocking this signal will make a real difference. This compelling need alongside recent drug innovations has propelled RAS research back to the forefront of cancer research[9]. Ongoing development of agents targeting $KRAS^{G12C}$ offers new hopes of precise treatment for $KRAS^{G12C}$-induced NSCLC[35,36]. In this work, we modified SAH-

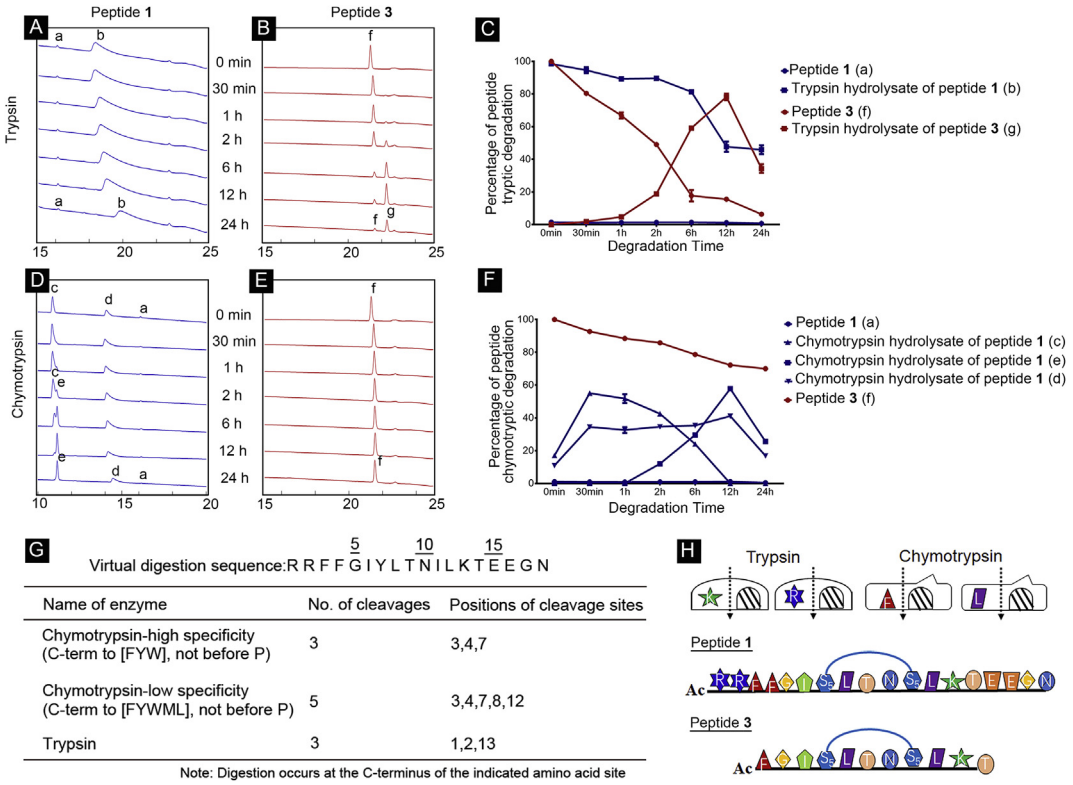

Name of enzyme	No. of cleavages	Positions of cleavage sites
Chymotrypsin-high specificity (C-term to [FYW], not before P)	3	3,4,7
Chymotrypsin-low specificity (C-term to [FYWML], not before P)	5	3,4,7,8,12
Trypsin	3	1,2,13

Note: Digestion occurs at the C-terminus of the indicated amino acid site

Figure 8 Enzymatic degradation of peptide **1** and **3.** (A)−(B) HPLC chromatograms of peptide **1** and **3** after 0, 30 min, 1, 2, 6, 12, and 24 h of tryptic degradation. (C) Percentage of peptides **1** and **3** and their trypsin hydrolysate at different time points. (D)−(E) HPLC chromatograms of peptides **1** and **3** after 0, 30 min, 1 2, 6, 12, and 24 h of α-chymotryptic degradation. (F) Percentage of peptides **1** and **3** and their chymotrypsin hydrolysate at different time points. (G) Virtual digestion on the amino acid sequence RRFFGIYLTNILKTEEGN with the PeptideCutter tool of ExPASy. (H) Schematic diagram of the amino acid sequences and enzyme active sites of peptides **1** and **3**. The data shown represent results of three individual experiments ($n = 3$).

$SOS1_A$ designed by Leshchiner et al.[18] to obtain shorter peptides with better stability. Among ten peptide candidates, we for the first time reported that peptide **3** induced cell death in KRAS mutant NSCLC cell line H358 in two ways: apoptosis and G2/M arrest. Peptide **3** also exerted strong anti-tryptic and anti-chymotryptic ability and bearded the plasma stability as well as human liver microsomal metabolic stability.

The activity of peptide has a certain correlation with its primary structure, namely the composition and sequence of amino acids. The C-terminus containing more hydrophobic amino acid residues and the N-terminus rich in basic amino acids are essential for activity. In addition, as far as the secondary structure of the peptide is concerned, the better α-helical conformation contributes to its better activity[37]. A typical α-helix consists of 12 amino acid residues, and a minimum of eight amino acid residues are required to complete an α-helix. Furthermore, if the peptide chain is too short, it is difficult to cross the activation energy barrier to form an α-helix. As the peptide chain gradually shortened in a series of stapled peptides designed in this paper, the hydrophobic amino acid residues at the C-terminus and the basic amino acids at the N-terminus were removed, and the number of amino acids was too short to form an α-helix, which were not conducive to their better activity. Generally, the higher the α-helicity of the peptide, the higher the affinity for the $KRAS^{G12C}$ protein. Although the affinity of the stapled peptide **3** to $KRAS^{G12C}$ protein is higher compared with the positive peptide **1**, it is not as strong as peptide **5** obtained by the D-type amino acid substitution we reported previously[38].

This is the first time that peptide **3** has been tested to inhibit the proliferation of lung cancer cells. The peptides **1** and **3** were comparable in proliferation inhibition in H358 cells. Cell cycle progression, an essential process supporting cell proliferation, is regulated by cell-cycle related proteins[31]. The stapled peptide **3** caused H358 cells G2/M cell cycle arrest, which might be attributed to the downregulation of cyclin B1 and CDK1 expression. As cell-cycle progression was blocked at the G2/M phase, cells may subsequently undergo apoptosis. It is one of the critical mechanisms of cancer cell death induced by cancer therapy[31,39−41]. Cancer cells often seek a balance between the pro-apoptotic protein and the anti-apoptotic protein to sustain cell viability. So BCL-2 or BAX inhibition that disturbs the balance is the key to trigger apoptosis. Furthermore, we tested the effect of peptide **3** on the phosphorylation of ERK in H358 cells using Western blot to determine whether the peptide **3**-induced inhibition on H358 cell viability observed was KRAS-dependent. As expected, peptide **3** dose-responsively inhibited ERK1/2 phosphorylation. And the results of genomics analysis and quantitative proteomics analysis further confirmed that peptide **3** can induce cell cycle arrest and apoptosis to inhibit H358 cell growth *via* disrupting the KRAS-mediated signaling pathway.

The development of inhibitors targeting the RAS protein has always been challenging. The earliest peptide-based RAS

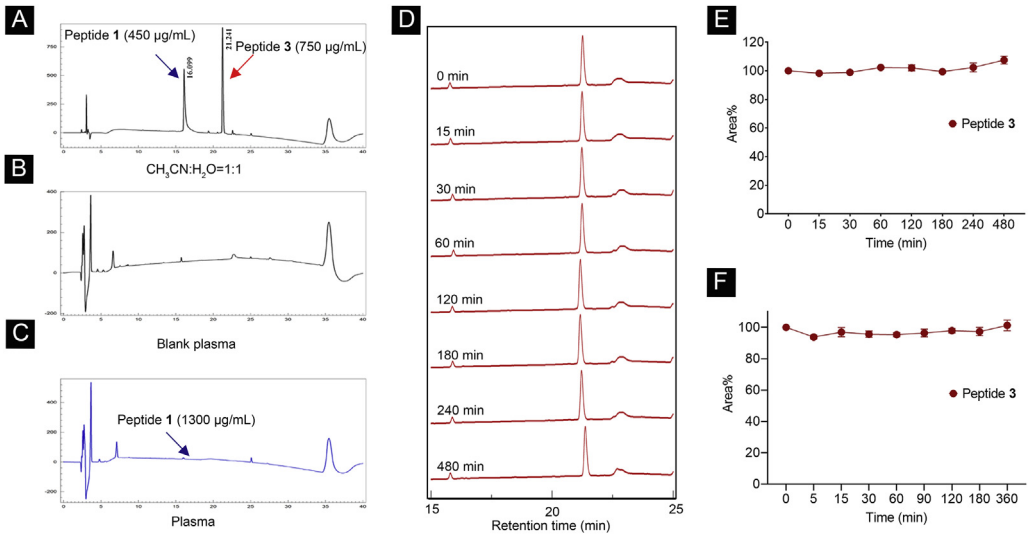

Figure 9 Plasma stability and metabolic stability of human liver microsomes of peptide **3.** (A) The HPLC chromatograms of peptides **1** and **3** with acetonitrile-water (1:1) mobile phases containing 0.1% formic acid. The blue arrow marks the characteristic peak of peptide **1**, and the red arrow indicates the characteristic peak of peptide **3.** (B) The chromatograms of blank plasma samples. (C) Peptide **1** (1300 μg/mL) in the plasma at 0 min. (D) Peptide **3** (500 μg/mL) in the plasma at 0, 15, 30, 60, 120, 180, 240, 480 min. (E) Changes in the peak area of peptide **3** within 480 min in the plasma. (F) Changes in the peak area of peptide **3** within 360 min in the human liver microsomes. The data shown represent results of three individual experiments ($n = 3$).

inhibitors were discovered by Clark et al.[42], whose mechanism was to block RAS-effector interaction *in vitro*. Since then, many peptide inhibitors with the same mechanism have been discovered, such as compound **12**[43], KD2[44], Cyclorasin 9A5[45], etc. In addition, peptide inhibitors such as HBS3 discovered by Patgiri et al.[19] could interfere with RAS–SOS interaction. However, there are some problems with peptide inhibitors, such as short half-life, poor stability, easy degradation by proteases, etc. The stapled peptide **3** with the mechanism of inhibiting SOS-mediated nucleotide association, showed excellent enzymatic stability, plasma stability and human liver microsomal metabolic stability. The presence of hydrocarbon stapling on the side chain slows the kinetics of proteolytic digestion. Thus, the possibility can be ruled out that the sites between the stapling amino acids or the adjacent amino acid are attacked by trypsin or chymotrypsin[40]. Because the protease requires the peptides to adopt an extended conformation to hydrolyze the amide bonds, the enhanced α-helix structures can render the peptides protease-resistant[25,46–48]. Peptides are mainly eliminated by non-specific enzymatic hydrolysis, such as proteolysis, gastrointestinal elimination, kidney elimination, and liver elimination, etc., with extensive metabolic sites and extremely low excretion of prototype drugs. There are mainly oxidation, reduction and hydrolysis reactions in the phase I metabolic reaction, the stapled peptide is metabolized by liver microsomes very little or not, which may account for the result that peptide **3** was relatively stable in liver microsomes.

Our study demonstrates that the stapled peptide **3** exhibits a stable α-helical structure with improved affinity and stability, strong resistance to proteolysis, and enhanced biological activity. The stapled peptide **3** provides a practical approach for polypeptide drug research, particularly for studies of more in-depth design of peptidomimetics and non-peptide drugs. The future experiments will focus on optimizing the potency of peptide **3** by using the analysis of structure–activity relationships and advancing it to preclinical testing of peptide **3** in murine models of KRAS-driven cancers. Our discovery will encourage the development of novel drugs for inhibition of KRAS mutations[49].

4. Experimental

4.1. *Expression and purification of KRAS^{G12C} protein*

The *Escherichia coli* Arctic-Express™ strain carrying the pCzn1-His vector was used as the expression host for hexahistidine-tagged recombinant human KRAS^{G12C}. After the bacterial growth to a certain density in Luria–Bertani medium at 37 °C, induction was performed at 11 °C with 0.5 mmol/L isopropyl-β-D-thiogalactoside, and then incubated overnight at 11 °C. After centrifugation to collect bacteria, the obtained pellet was resuspended in lysis buffer containing protease inhibitors, followed by ultrasonic lysis and centrifugation again. The concentration of the protein purified *via* Ni-affinity resin was determined by the BCA assay.

4.2. *Synthesis and purification of stapled peptides*

Rink amide 4-methyl-benzhydryl amine resin (0.57 mmol/g) was applied to the synthesis of stapled peptides. Activate Fmoc-protected amino acids with 1-hydroxybenzotriazole (HOBt), *o*-benzotriazol-1-yl-*N*,*N*,*N*′,*N*′-tetramethyluronium hexafluorophosphate (HBTU), and *N*,*N*-diisopropylethylamine (DIEA) in dichloromethane (DCM) before being added into rink resin. After completing the coupling reaction, wash resin with dimethyl formamide (DMF) and DCM. Other amino acids were then coupled to the peptide sequentially. Coupling and deprotection cycles of steps were carried out in a peptide synthesizer. Adding the Grubbs 2nd-generation catalyst in dichloroethane (DCE) into the peptidyl-resin and the suspension was kept for 2 h at 45 °C. After filtering the mixture, the metathesis reaction was desirable to be repeated twice or more, followed by washing with DCE and MeOH. Remove the Fmoc group before the

Table 3 Purity and LC–MS/MS spectrometry data for the stapled peptides.

Peptide	Molecular formula	Calcd. mass $[M+H]^+$	Found	Purity (%)
1	$C_{100}H_{159}N_{27}O_{28}$	2187.17	2187.06	98.9
2	$C_{77}H_{119}N_{15}O_{20}$	1574.83	1574.06	97.1
3	$C_{63}H_{103}N_{13}O_{16}$	1298.54	1297.82	95.8
4	$C_{50}H_{87}N_{11}O_{13}$	1050.02	1049.89	94.8
5	$C_{42}H_{72}N_8O_{11}$	864.78	864.61	99.7
6	$C_{30}H_{50}N_6O_9$	638.44	638.48	90.5
7	$C_{52}H_{91}N_{11}O_{14}$	1094.07	1094.17	97.8
8	$C_{46}H_{80}N_{10}O_{13}$	980.90	980.95	95.2
9	$C_{53}H_{84}N_{10}O_{13}$	1069.02	1068.87	98.3
10	$C_{47}H_{73}N_9O_{12}$	955.85	955.80	92.5

peptide was capped by acetylation. Side chain protecting groups of amino acids were removed before peptides cleaved from the resin using trifluoroacetic acid (TFA)/H_2O/phenol/triisopropylsilyl chloride (TIS). Crude peptides were then precipitated with cold ether and subsequently centrifuged, and further purified by preparative C18 reversed-phase HPLC. The purity of all stapled peptides was purified to more than 90% and further confirmed by LC–MS/MS and analytical HPLC. Purity and LC–MS/MS spectrometry data for the stapled peptides were in Table 3. HPLC reports, peak tables, and MS reports of stapled peptides were in Supporting Information.

4.3. Circular dichroism spectroscopy

To estimate the secondary structure of the polypeptide, analysis of CD spectrum was performed on a J-810 spectrometer (Jasco, Japan) at 25 °C using a quartz cell with a path length of 1.0 mm, and the absorbance at 190−260 nm was recorded (bandwidth: 1 nm; scan speed: 50 nm/min; response time: 1 s). The stapled peptides were respectively dissolved in phosphate buffer solution (PBS, pH 7.4) and PBS (50% trifluoroethanol, pH 7.4) to prepare a peptide solution at a concentration of 0.3 mg/mL. Each spectrum for data analysis was an average of three readings. The resulting CD spectra were converted to mean residue ellipticity θ (deg × cm^2/dmol) *versus* wavelength λ (nm).

4.4. Biolayer interferometry

Biolayer interferometry experiments were performed according to our previous experimental methods[38]. The binding kinetic constants of stapled peptides to $KRAS^{G12C}$ protein were performed by ForteBio Octet RED 96 system. First, incubate $KRAS^{G12C}$ protein with biotin and the stapled peptides were diluted into various concentrations. Finally, calculate the K_D values through the SSA sensor (Fortebio).

4.5. Fluorescence polarization assay

The binding experiments were performed on a SpectraMax MultiMode Microplate Reader (Molecular Devices) with excitation wavelength at 485 nm and emission wavelength at 535 nm, respectively. In the FP assays, FP was determined by measuring the parallel and perpendicular fluorescence intensities (F$\parallel$ and F$\perp$). Firstly, the concentration of FITC-Peptide-**1** and FITC-Peptide-**3** were optimized and then FITC-Peptide-**1** and FITC-Peptide-**3** peptides were incubated with the indicated serial dilution of $KRAS^{G12C}$ protein in PBS (pH 8.0) until equilibrium was reached (30 min). EC_{50} values were calculated by nonlinear regression analysis of dose−response curves using Prism software (GraphPad).

4.6. Docking

The positive peptide **1** and the stapled peptide **3** were constructed by Accelrys Discovery Studio (DS) 3.0 (Accelrys, Inc., San Diego, CA, USA). Peptide **1** and peptide **3** were respectively docked to target protein (PDB ID: 6EPL) through the CDOCKER (DS 3.0)[11].

4.7. Nucleotide association assay

The association of 2′-/3′-*O*-(*N*′-methylcarbamoyl) guanosine-5′-*O*-diphosphate (mant-GDP) with $KRAS^{G12C}$ protein was monitored by fluorescence measurement over time on a Molecular Devices iD5 Multi-Function Microplate Reader (excitation 355 nm, emission 448 nm). Different concentrations of peptides were incubated with $KRAS^{G12C}$ protein and mant-GDP (Sigma, St. Louis, MO, USA) in buffer containing 25 mmol/L Tris (pH 7.5), 50 mmol/L NaCl, and 1 mmol/L D,L-dithiothreitol (DTT) at 25 °C, the final concentration of $KRAS^{G12C}$ protein and mant-GDP both were 1 μmol/L. $KRAS^{G12C}$ protein and mant-GDP alone established the positive control for association, and competition with 200-fold excess unlabeled GDP (Sigma) served as the negative control.

4.8. Cell culture

H358 cells were purchased from the Cell Bank of Shanghai. RPMI-1640 medium (Gibco, Grand Island, NY, USA) containing 10% fetal bovine serum, 100 units/mL penicillin, and 100 mg/mL streptomycin (Sigma) was applied to cells culture in a humidified atmosphere with 5% CO_2 at 37 °C.

4.9. Cell viability assay

The cell viability of H358 cells bearing $KRAS^{G12C}$ mutation was examined by Cell Counting Kit-8 (CCK8) assay. Cells were cultured in a 96-well plate overnight before a 24-h incubation with various concentrations of synthesized peptides. After adding

CCK8 solution (Beyotime, Shanghai, China) to each well, the plates were placed for another 1 h at 37 °C. Measure the absorbance at 450 nm on Multiskan FC microplate reader. In addition, cell viability of H358 cells after 36-, 48-, and 72-h incubation with a diluted series of peptide **3** was examined by CCK8 assay.

4.10. Cell cycle analysis

H358 cells were seeded onto 6-well plates and treated with peptides for another 24 h. The cells were collected and then fixed with ethanol. After that, the cells were resuspended in propidium iodide (PI) staining solution (Beyotime). For each sample, 10,000 cells were analyzed through flow cytometry (MACSQuant, Miltenyi Biotec GmbH), and the proportion of cells in each cell-cycle phases were determined with Flow Jo7.6.1 software.

4.11. Annexin V-FITC apoptosis assay

The apoptotic cells induced by peptides were determined by flow-cytometry (MACSQuant, Miltenyi Biotec GmbH). H358 cells were treated with peptides and digested with trypsin. Apoptosis assay was performed on H358 cells with Annexin V-FITC Apoptosis Detection kit (Beyotime). At least 10,000 events were collected and analyzed for Annexin V-FITC staining. The proportion of Annexin V-positive apoptotic cells was calculated in Flow Jo_V10 software.

4.12. Western blot

H358 cells treated with peptides at different concentrations were collected and lysed by cell lysis buffer (Beyotime) containing Phosphatase Inhibitor Cocktail (Bimake) and protease inhibitor PMSF on ice for 1 h. SDS-PAGE was used to separate proteins and then transferred it onto PVDF membranes (Millipore, USA). After being blocked, incubate the membranes with primary antibody at 4 °C overnight followed by a 100-min incubation with HRP-labeled Goat Anti-Rabbit IgG (H + L) (Beyotime). Visualize protein bands on Molecular Imager ChemiDoc XRS + System (Bio Rad Laboratories, Inc.). Polyclonal anti-BAX (No. BTL0455T), anti-BCL-2 (No. BTL0470T), and anti-GAPDH (No.BTL3215M) antibodies were bought from Biotech Lab. Caspase-3 Antibody (#9662) and Cyclin B1 (D5C10) XP® Rabbit mAb (#12231) were provided by Cell Signaling Technology (Beverly, MA, USA). CDK1 Antibody (#48788), p44/42 MAP Kinase (Phospho-Thr202) Antibody (#11245), and ERK1/2 Antibody (#48616) were supplied by Signalway Antibody.

4.13. RNA-seq

H358 cells were treated with 20 μmol/L of peptide **3** or with equal volume of PBS as control, and were incubated in a humidified atmosphere of 5% CO_2 at 37 °C for 24 h. Cell samples were collected and added Trizol reagent (Invitrogen, CA, USA), and then handed over to LC-Bio Technology Co., Ltd. (Hangzhou, China) for the subsequent mRNA library construction and sequencing. StringTie and ballgown were used to estimate the expression levels of all transcripts and perform expression level for mRNAs by calculating FPKM. The differentially expressed mRNAs were selected with fold change >two or fold change <0.5 and P value < 0.05 by R package edgeR or DESeq2, and then analysis KEGG enrichment to the differentially expressed mRNAs.

4.14. Quantitative proteome analysis

H358 cells were treated with 20 μmol/L of peptide **3** or with equal volume of PBS as control, and were incubated in a humidified atmosphere of 5% CO_2 at 37 °C for 24 h. Cell samples were collected and then handed over to LC-Bio Technology Co., Ltd. for the subsequent proteome analysis with TMT technology. Quantitative proteome analysis involved the following six steps in turn: sample preparation, SDS-PAGE separation, filter-aided sample preparation (FASP Digestion), TMT labeling, peptide fractionation with reversed phase chromatography, and mass spectrometry analysis. MS/MS raw files were processed using MASCOT engine (Matrix Science, London, UK; version 2.6) embedded into Proteome Discoverer 2.2, and searched against the Protein Database for peptide identification. A peptide and protein false discovery rate of 1% was enforced using a reverse database search strategy. Proteins with Fold change >1.2 and P value (Student's t-test) < 0.05 were considered to be differentially expressed proteins, which were subjected to GO and KEGG analysis.

4.15. Enzymatic degradation

Enzymatic degradation of stapled peptides by trypsin (MACKLIN, Shanghai, China) and chymotrypsin (MACKLIN) was carried out using 150 μg/mL of peptide and 3 μg/mL of the enzyme (peptide-to-enzyme weight ratio of 50:1) in NH_4HCO_3 buffer at 37 °C. Samples were collected at different time points. 1% (*v*/*v*) formic acid was used to shut down the enzymatic reaction. Samples were then analyzed by Shimadzu HPLC. The chromatographic separation was conducted on a Thermo Scientific™ Syncronis™ C18 column (250 mm × 4.6 mm, 5 μm) with a gradient mobile phase that solvent A was 0.1% trifluoroacetate acid in water and solvent B was 0.1% trifluoroacetate acid in acetonitrile. Following is the gradient program: 0 min 20% solvent B; 30 min 90% solvent B; 31 min 20% solvent B; 40 min 20% solvent B. The flow rate was 1 mL/min, with an injection volume of 20 μL.

4.16. Plasma stability

A certain amount of heparin sodium solution was added to a blood collection tube, and the blank blood was sampled from the femoral artery from Sprague−Dawley rats. Matrix-present samples were prepared by centrifugation at 4 °C and 4000 r/min for 10 min. Rat plasma was mixed with stapled peptides solution to a concentration of 500 μg/mL. The mixture was then incubated at 37 °C. An aliquot of 50 μL solution was pipetted into 150 μL of methanol-acetonitrile (50:50, *v*/*v*) at a different time interval to precipitate plasma proteins. After vortex and centrifugation, the supernatant was determined by Shimadzu HPLC. The specific chromatographic separation procedure was the same as Section 4.15.

4.17. Human liver microsome assay

Phase I metabolic stability kit was purchased from Beijing Huizhi Taikang Pharmaceutical Technology Co., Ltd. Thawed the components of the kit in an ice bath and place them on ice for later use; excepted for the human liver microsomes, mixed the other components of the incubation system according to the instructions (200 μL incubation system contained 10 μL solution A (20 ×), two μL solution B (100 ×), and 182 μL 0.1 mol/L PBS buffer, the final

concentration of peptide was 100 μmol/L), and the mixture was pre-incubated at 37 °C for 5 min; added 5 μL human liver microsomes (20 mg/mL) to start the metabolic reaction at 37 °C in a water bath after mixing; at the set incubation time point, the termination solution was added to the incubation system to terminate the reaction (such as pre-cooled acetonitrile, $V_{\text{Pre-cooled acetonitrile}}/V_{\text{Incubation system}} = 1{:}1$). After vortex and centrifugation, the supernatant was determined by Shimadzu HPLC. The specific chromatographic separation procedure was the same as Section 4.15.

4.18. Statistical analyses

GraphPad Prism 8.4.2 and SPSS 23.0 software were used for the statistical analyses. All data were analyzed using a one-way ANOVA. Descriptive data were represented as the mean ± standard deviation (SD). For all tests, only a P value < 0.05 was considered statistically significant.

Acknowledgments

This study was supported by projects of the National Natural Science Foundation of China (81803354 and 81773693); the Natural Science Foundation of Jiangsu Province of China (BK20180564); the Fundamental Research Funds for the Central Universities (2632021ZD13, China); Double First-Class Innovation Team of China Pharmaceutical University (CPU2018GY02, China); the Program for Outstanding Scientific and Technological Innovation Team of Jiangsu Higher Education (YY20180315004, China).

Author contributions

The manuscript was written with contributions from all authors. All authors have given approved the final version of the manuscript. Lili Xu and Cuicui Li designed the research. Cuicui Li, Ni Zhao, Luyan An, Zhen Dai, Xiaoyi Chen, and Fan Yang performed the experiments of this study. Lili Xu and Cuicui Li wrote the original draft. Chi Hu, Bin Di, and Qidong You reviewed and edited the paper.

Conflicts of interest

The authors declare no conflicts of interest.

Appendix A. Supporting information

Supporting information to this article can be found online at https://doi.org/10.1016/j.apsb.2021.06.013.

References

1. Cheng H, Planken S. Precedence and promise of covalent inhibitors of EGFR and KRAS for patients with non-small-cell lung cancer. *ACS Med Chem Lett* 2018;**9**:861−3.
2. Wang JB, Huang X, Li FR. Impaired dendritic cell functions in lung cancer: a review of recent advances and future perspectives. *Cancer Commun (Lond)* 2019;**39**:43.
3. Zhang P, Ma J, Zhang Q, Jian S, Sun X, Liu B, et al. Monosaccharide analogues of anticancer peptide R-lycosin-I: role of monosaccharide conjugation in complexation and the potential of lung cancer targeting and therapy. *J Med Chem* 2019;**62**:7857−73.
4. Jemal A, Bray F, Center MM, Ferlay J, Ward E, Forman D. Global cancer statistics. *CA Cancer J Clin* 2011;**61**:69−90.
5. Li S, Liu S, Deng J, Akbay EA, Hai J, Ambrogio C, et al. Assessing therapeutic efficacy of MEK inhibition in a KRAS(G12C)-driven mouse model of lung cancer. *Clin Cancer Res* 2018;**24**:4854−64.
6. Prior IA, Lewis PD, Mattos C. A comprehensive survey of Ras mutations in cancer. *Cancer Res* 2012;**72**:2457−67.
7. De Castro Carpeño J, Belda-Iniesta C. KRAS mutant NSCLC, a new opportunity for the synthetic lethality therapeutic approach. *Transl Lung Cancer Res* 2013;**2**:142−51.
8. Rothschild SI. Targeted therapies in non-small cell lung cancer-beyond EGFR and ALK. *Cancers (Basel)* 2015;**7**:930−49.
9. Thomas JC, Cooper JM, Clayton NS, Wang C, White MA, Abell C, et al. Inhibition of Ral GTPases using a stapled peptide approach. *J Biol Chem* 2016;**291**:18310−25.
10. Trinh TB, Upadhyaya P, Qian Z, Pei D. Discovery of a direct ras inhibitor by screening a combinatorial library of cell-permeable bicyclic peptides. *ACS Comb Sci* 2016;**18**:75−85.
11. Hillig RC, Sautier B, Schroeder J, Moosmayer D, Hilpmann A, Stegmann CM, et al. Discovery of potent SOS1 inhibitors that block RAS activation *via* disruption of the RAS–SOS1 interaction. *Proc Natl Acad Sci U S A* 2019;**116**:2551−60.
12. Guillard S, Kolasinska-Zwierz P, Debreczeni J, Breed J, Zhang J, Bery N, et al. Structural and functional characterization of a DARPin which inhibits ras nucleotide exchange. *Nat Commun* 2017;**8**:16111.
13. Christensen JG, Olson P, Briere T, Wiel C, Bergo MO. Targeting Kras(g12c)-mutant cancer with a mutation-specific inhibitor. *J Intern Med* 2020;**288**:183−91.
14. Hallin J, Engstrom LD, Hargis L, Calinisan A, Aranda R, Briere DM, et al. The KRAS(G12C) inhibitor MRTX849 provides insight toward therapeutic susceptibility of KRAS-mutant cancers in mouse models and patients. *Cancer Discov* 2020;**10**:54−71.
15. Li FY, Zhang ZF, Voss S, Wu YW, Zhao YF, Li YM, et al. Inhibition of K-Ras4B-plasma membrane association with a membrane microdomain-targeting peptide. *Chem Sci* 2020;**11**:826−32.
16. Hunter JC, Manadhar A, Carrasco MA, Gurbani D, Gondi S, Westover KD. Biochemical and structural analysis of common cancer-associated KRAS mutations. *Mol Cancer Res* 2015;**13**:1325−35.
17. Bos JL, Rehmann H, Wittinghofer A. GEFs and GAPs: critical elements in the control of small G proteins. *Cell* 2007;**129**:865−77.
18. Leshchiner ES, Parkhitko A, Bird GH, Luccarelli J, Bellairs JA, Escudero S, et al. Direct inhibition of oncogenic KRAS by hydrocarbon-stapled SOS1 helices. *Proc Natl Acad Sci U S A* 2015;**112**:1761−6.
19. Patgiri A, Yadav KK, Arora PS, Bar-Sagi D. An orthosteric inhibitor of the Ras–Sos interaction. *Nat Chem Biol* 2011;**7**:585−7.
20. Li B, Yang XX, Li L. Research progress in the synthesis and bioactivity of stapled peptide. *Acta Pharm Sin* 2017;**52**:685−98.
21. Tan YS, Lane DP, Verma CS. Stapled peptide design: principles and roles of computation. *Drug Discov Today* 2016;**21**:1642−53.
22. Wallbrecher R, Chene P, Ruetz S, Stachyra T, Vorherr T, Brock R. A critical assessment of the synthesis and biological activity of p53/human double minute 2-stapled peptide inhibitors. *Br J Pharmacol* 2017;**174**:2613−22.
23. Verdine GL, Hilinski GJ. Stapled peptides for intracellular drug targets. *Methods Enzymol* 2012;**503**:3−33.
24. Long YQ, Huang SX, Zawahir Z, Xu ZL, Li H, Sanchez TW, et al. Design of cell-permeable stapled peptides as HIV-1 integrase inhibitors. *J Med Chem* 2013;**56**:5601−12.
25. Moiola M, Memeo MG, Quadrelli P. Stapled peptides-a useful improvement for peptide-based drugs. *Molecules* 2019;**24**:3654.
26. Serrano JC, Sipthorp J, Xu W, Itzhaki LS, Ley SV. A new methodology for incorporating chiral linkers into stapled peptides. *Chembiochem* 2017;**18**:1066−71.
27. Lamberts SWJ, Hofland LJ. Anniversary review: octreotide, 40 years later. *Eur J Endocrinol* 2019;**181**:R173−83.
28. Kim YW, Grossmann TN, Verdine GL. Synthesis of all-hydrocarbon stapled alpha-helical peptides by ring-closing olefin metathesis. *Nat Protoc* 2011;**6**:761−71.

29. Gade TP, Hassen W, Santos E, Gunset G, Saudemont A, Gong MC, et al. Targeted elimination of prostate cancer by genetically directed human T lymphocytes. *Cancer Res* 2005;**65**:9080−8.
30. Ryan MB, Fece De La Cruz F, Phat S, Myers DT, Wong E, Shahzade HA, et al. Vertical pathway inhibition overcomes adaptive feedback resistance to KRAS(G12C) inhibition. *Clin Cancer Res* 2020;**26**:1633−43.
31. Luo LX, Li Y, Liu ZQ, Fan XX, Duan FG, Li RZ, et al. Honokiol induces apoptosis, G1 arrest, and autophagy in KRAS mutant lung cancer cells. *Front Pharmacol* 2017;**8**:199.
32. Chang CY, Lin CW, Chiang SK, Chen PL, Huang CY, Liu SJ, et al. Enzymatic stability and immunoregulatory efficacy of a synthetic indolicidin analogue with regular enantiomeric sequence. *ACS Med Chem Lett* 2013;**4**:522−6.
33. Schreier VN, Mezo G, Orban E, Durr C, Marquardt A, Manea M. Synthesis, enzymatic stability and *in vitro* cytostatic effect of Daunorubicin-GnRH-III derivative dimers. *Bioorg Med Chem Lett* 2013;**23**:2145−50.
34. Osapay K, Tran D, Ladokhin AS, White SH, Henschen AH, Selsted ME. Formation and characterization of a single Trp-Trp cross-link in indolicidin that confers protease stability without altering antimicrobial activity. *J Biol Chem* 2000;**275**:12017−22.
35. Janes MR, Zhang J, Li LS, Hansen R, Peters U, Guo X, et al. Targeting KRAS mutant cancers with a covalent G12C-specific inhibitor. *Cell* 2018;**172**:578−89.
36. Liu M, Sjogren AKM, Karlsson C, Ibrahim MX, Andersson KME, Olofsson FJ, et al. Targeting the protein prenyltransferases efficiently reduces tumor development in mice with K-RAS-induced lung cancer. *Proc Natl Acad Sci U S A* 2010;**107**:6471−6.
37. Bullock BN, Jochim AL, Arora PS. Assessing helical protein interfaces for inhibitor design. *J Am Chem Soc* 2011;**133**:14220−3.
38. Xu LL, Li CC, An LY, Dai Z, Chen XY, You QD, et al. Selective apoptosis-inducing activity of synthetic hydrocarbon-stapled SOS1 helix with D-amino acids in H358 cancer cells expressing KRAS(G12C). *Eur J Med Chem* 2020;**185**:111844.
39. Mcnew KL, Whipple WJ, Mehta AK, Grant TJ, Ray L, Kenny C, et al. MEK and TAK1 regulate apoptosis in colon cancer cells with KRAS-dependent activation of proinflammatory signaling. *Mol Cancer Res* 2016;**14**:1204−16.
40. Dougherty PG, Wen J, Pan X, Koley A, Ren JG, Sahni A, et al. Enhancing the cell permeability of stapled peptides with a cyclic cell-penetrating peptide. *J Med Chem* 2019;**62**:10098−107.
41. Rezaei Araghi R, Bird GH, Ryan JA, Jenson JM, Godes M, Pritz JR, et al. Iterative optimization yields Mcl-1-targeting stapled peptides with selective cytotoxicity to Mcl-1-dependent cancer cells. *Proc Natl Acad Sci U S A* 2018;**115**:E886−95.
42. Clark GJ, Drugan JK, Terrell RS, Bradham C, Der CJ, Bell RM, et al. Peptides containing a consensus Ras binding sequence from Raf-1 and theGTPase activating protein NF1 inhibit Ras function. *Proc Natl Acad Sci U S A* 1996;**93**:1577−81.
43. Wu X, Upadhyaya P, Villalona-Calero MA, Briesewitz R, Pei D. Inhibition of Ras-effector interaction by cyclic peptides. *Medchemcomm* 2013;**4**:378−82.
44. Zhang Z, Gao R, Hu Q, Peacock H, Peacock DM, Dai S, et al. GTP-state-selective cyclic peptide ligands of K-Ras(G12D) block its interaction with Raf. *ACS Cent Sci* 2020;**6**:1753−61.
45. Upadhyaya P, Qian Z, Selner NG, Clippinger SR, Wu Z, Briesewitz R, et al. Inhibition of Ras signaling by blocking Ras–effector interactions with cyclic peptides. *Angew Chem Int Ed Engl* 2015;**54**:7602−6.
46. Bird GH, Madani N, Perry AF, Princiotto AM, Supko JG, He XY, et al. Hydrocarbon double-stapling remedies the proteolytic instability of a lengthy peptide therapeutic. *Proc Natl Acad Sci U S A* 2010;**107**:14093−8.
47. Bann SJ, Ballantine RD, Mccallion CE, Qian PY, Li YX, Cochrane SA. A chemical-intervention strategy to circumvent peptide hydrolysis by D-stereoselective peptidases. *J Med Chem* 2019;**62**:10466−72.
48. Ruiz-Santaquiteria M, De Castro S, Toro MA, De Lucio H, Gutierrez KJ, Sanchez-Murcia PA, et al. Trypanothione reductase inhibition and anti-leishmanial activity of all-hydrocarbon stapled alpha-helical peptides with improved proteolytic stability. *Eur J Med Chem* 2018;**149**:238−47.
49. Han CW, Jeong MS, Ha SC, Jang SB. A H-REV107 peptide inhibits tumor growth and interacts directly with oncogenic KRAS mutants. *Cancers (Basel)* 2020;**12**:1412.
50. Uprety D, Adjei AA. KRAS: From undruggable to a druggable cancer target. *Cancer Treat Rev* 2020;**89**:102070.
51. Chen H, Smaill JB, Liu TZ, Ding K, Lu XY. Small-molecule inhibitors directly targeting KRAS as anticancer therapeutics. *J Med Chem* 2020;**63**:14404−24.
52. Chen SJ, Li FY, Xu D, Hou K, Fang WR, Li YM. The function of RAS mutation in cancer and advances in its drug research. *Curr Pharm Design* 2019;**25**:1105−14.